Biomaterials 34 (2013) 1033–1040

Contents lists available at SciVerse ScienceDirect

Biomaterials

journal homepage: www.elsevier.com/locate/biomaterials

Hydrogels derived from central nervous system extracellular matrix

Christopher J. Medberry [a,c,1], Peter M. Crapo [c,1], Bernard F. Siu [a,c], Christopher A. Carruthers [a,c], Matthew T. Wolf [a,c], Shailesh P. Nagarkar [d], Vineet Agrawal [c,e], Kristen E. Jones [c], Jeremy Kelly [c], Scott A. Johnson [c], Sachin S. Velankar [d], Simon C. Watkins [f], Michel Modo [a,c], Stephen F. Badylak [b,c,*]

[a] Department of Bioengineering, University of Pittsburgh, Pittsburgh, PA 15219, USA
[b] Department of Surgery, University of Pittsburgh, Pittsburgh, PA 15213, USA
[c] McGowan Institute for Regenerative Medicine, University of Pittsburgh, Pittsburgh, PA 15219, USA
[d] Department of Chemical Engineering, University of Pittsburgh, Pittsburgh, PA 15261, USA
[e] Medical Scientist Training Program, University of Pittsburgh School of Medicine, Pittsburgh, PA 15261, USA
[f] Department of Cell Biology and Physiology, Center for Biological Imaging, University of Pittsburgh, Pittsburgh, PA 15261, USA

ARTICLE INFO

Article history:
Received 29 August 2012
Accepted 25 October 2012
Available online 16 November 2012

Keywords:
ECM (extracellular matrix)
Hydrogel
Scaffold
Central nervous system
Regenerative medicine
Tissue engineering

ABSTRACT

Biologic scaffolds composed of extracellular matrix (ECM) are commonly used repair devices in preclinical and clinical settings; however the use of these scaffolds for peripheral and central nervous system (CNS) repair has been limited. Biologic scaffolds developed from brain and spinal cord tissue have recently been described, yet the conformation of the harvested ECM limits therapeutic utility. An injectable CNS-ECM derived hydrogel capable of in vivo polymerization and conformation to irregular lesion geometries may aid in tissue reconstruction efforts following complex neurologic trauma. The objectives of the present study were to develop hydrogel forms of brain and spinal cord ECM and compare the resulting biochemical composition, mechanical properties, and neurotrophic potential of a brain derived cell line to a non-CNS-ECM hydrogel, urinary bladder matrix. Results showed distinct differences between compositions of brain ECM, spinal cord ECM, and urinary bladder matrix. The rheologic modulus of spinal cord ECM hydrogel was greater than that of brain ECM and urinary bladder matrix. All ECMs increased the number of cells expressing neurites, but only brain ECM increased neurite length, suggesting a possible tissue-specific effect. All hydrogels promoted three-dimensional uni- or bipolar neurite outgrowth following 7 days in culture. These results suggest that CNS-ECM hydrogels may provide supportive scaffolding to promote in vivo axonal repair.

1. Introduction

Biologic scaffolds composed of extracellular matrix (ECM) can facilitate the constructive remodeling of numerous tissues including esophagus [1,2], lower urinary tract [3,4], muscle and tendon [5,6], and myocardium [7,8], among others. Although the mechanisms by which ECM scaffolds promote a constructive and functional remodeling response are only partially understood, recruitment of endogenous multipotent progenitor cells [9,10], modulation of the innate immune response [11,12], scaffold degradation with the generation of bioactive molecular cues [13–15], and innervation [16] have all been shown to be important events in this process. The contribution of the innate three-dimensional ultrastructure, unique surface ligand distribution, or molecular composition to constructive, functional remodeling is largely unknown. However, hydrogel formulations of matrix scaffolds lack the native three-dimensional ultrastructure of the source tissue but still possess in vitro and in vivo biologic activity [17–22], suggesting that the molecular composition of these materials is an active factor in remodeling events. There have also been reports that suggest tissue-specific biologic scaffold materials have properties that enhance greater site-appropriate phenotypic cell differentiation compared to ECM scaffolds derived from non-homologous tissue sources [23–26].

The use of biologic scaffold materials within either the central or peripheral nervous system has not been extensively investigated [27]. However, it has been shown that innervation of remodeled scaffold materials is an early event when such materials are placed in several different anatomic locations and represents a predictor of

* Corresponding author. McGowan Institute for Regenerative Medicine, University of Pittsburgh, Pittsburgh, PA 15219, USA. Tel.: +1 412 235 5144; fax: +1 412 235 5110.
E-mail address: badylaks@upmc.edu (S.F. Badylak).
[1] These authors contributed equally to this work.

0142-9612/$ – see front matter © 2012 Elsevier Ltd. All rights reserved.
http://dx.doi.org/10.1016/j.biomaterials.2012.10.062

constructive and functional outcomes [16,28,29]. It has also been shown that innervation is a critical event in robust regenerative responses that occur in species such as the newt and axolotl [30–32]. Methods for the isolation of central nervous system (CNS) ECM have recently been described. The objectives of the present study were to develop a method to create hydrogel forms of brain and spinal cord ECM, examine the biomolecular composition and mechanical properties of the resulting hydrogels, and evaluate the in vitro neural cytocompatibility and neurotrophic potential of CNS-ECM hydrogels versus a hydrogel prepared from a non-CNS-ECM; specifically, porcine urinary bladder matrix.

2. Materials and methods

2.1. Overview of experimental design

Following decellularization of porcine brain and spinal cord, the resulting brain and spinal cord ECM (B-ECM and SC-ECM, respectively) were solubilized. The ECM materials were analyzed for collagen and sulfated glycosaminoglycan content, ultrastructure, and hydrogel mechanical properties. A commonly used neural cell line for examining neurite extension, N1E-115 [33,34], was used to identify the neurotrophic potential of ECM hydrogels in two- and three-dimensional culture. The results were compared to an ECM hydrogel manufactured from a non-CNS source, porcine urinary bladder matrix (UBM-ECM) [20].

2.2. ECM biologic scaffold production

Porcine brain, spinal cord, and urinary bladder were obtained from market weight animals (Tissue Source, Lafayette, IN). Tissues were frozen immediately after harvesting at −80 °C, thawed before use, and processed by tissue-specific methods described previously (Table 1A) [23]. In brief, CNS tissue was agitated (spinal cord tissue at 200 rpm; brain tissue at 120 rpm unless otherwise stated) in the following decellularization baths: deionized water (16 h at 4 °C; 60 rpm), 0.02% trypsin/0.05% EDTA (60 min at 37 °C; 60 rpm; Invitrogen Corp., Carlsbad, CA, USA), 3.0% Triton X-100 (60 min; Sigma–Aldrich Corp., St. Louis, MO, USA), 1.0 M sucrose (15 min; Fisher Scientific, Pittsburgh, PA, USA), water (15 min), 4.0% deoxycholate (60 min; Sigma), 0.1% peracetic acid (Rochester Midland Corp., Rochester, NY, USA) in 4.0% ethanol (v/v; 120 min), PBS (15 min; Fisher), deionized water (twice for 15 min each rinse), and PBS (15 min). Each bath was followed by rinsing the remaining tissue through a strainer with deionized water. Decellularized B-ECM and SC-ECM were lyophilized and stored dry until use.

UBM-ECM was prepared as previously described [35]. In brief, connective tissue was removed from the serosal surface of the bladder. The tunica serosa, tunica submucosa, and majority of the tunica muscularis mucosa were mechanically delaminated, which left the basement membrane and tunica propria intact. Luminal urothelial cells were dissociated from the basement membrane by soaking the UBM-ECM in deionized water. The UBM-ECM was then agitated in 0.1% peracetic acid in 4.0% ethanol (v/v; 120 min; 300 rpm) followed by a series of PBS and deionized water rinses and lyophilization.

2.3. ECM digestion and solubilization

Lyophilized and comminuted B-ECM (20 mesh), SC-ECM (20 mesh or hand cut), and UBM-ECM (20 mesh or hand cut; 400–1000 μm largest particle dimension as measured by mesh diameter or ruler) were separately placed into a 0.01 N HCl solution containing 1 mg/mL pepsin (Sigma) at a concentration of 10 mg ECM/mL and stirred at room temperature for 48 h as previously described (Table 1B) [20]. After 48 h, B-ECM, SC-ECM, and UBM-ECM were completely digested and formed a pre-gel solution (pH ~ 2). The pre-gel ECM solution was brought to pH 7.4 using 0.01 N NaOH and diluted to the desired volume/salt concentration using 10× and 1 × PBS. Pepsin is irreversibly inactivated at pH above 7.5 [36].

Table 1
Methods for decellularization and solubilizing B-ECM, SC-ECM, and UBM-ECM.

A. Decellularization methods		
Step	B-ECM and SC-ECM (120 and 180 rpm respectively)	UBM-ECM (300 rpm)
1.	Deionized water soak (18–24 h)	Mechanical delamination
2.	0.025% Trypsin (1 h)	
3.	3% Triton × 100 (1 h)	
4.	1 M Sucrose (30 min.)	
5.	Deionized water soak (30 min.)	
6.	4% Deoxycholic acid (1 h)	
7.	0.01% Peracetic acid	

B. Methods for solubilizing and digesting			
	B-ECM	SC-ECM	UBM-ECM
Particle size	<400 μm	400–1000 μm	
Solubilization	0.01 N HCl		
Digestion	1 mg/mL Pepsin		

2.4. Collagen and sGAG quantification

Collagen concentration of the pre-gel ECM solution was determined for samples from each production batch with the Sircol Assay Kit (Biocolor Ltd., UK) following the manufacturer's recommended protocol ($n = 4$ in duplicate or triplicate). Sulfated glycosaminoglycan (sGAG) concentrations were determined using digested ECM at a concentration of 50 mg ECM/ml with 0.1 mg/ml proteinase K (Sigma) in buffer (10 mM Tris–HCl, pH 8.0, 100 mM NaCl, 25 mM EDTA for 48–72 h at 50 °C) using the Blyscan Sulfated Glycosaminoglycan Assay Kit (Biocolor Ltd., UK) and following the manufacturer's recommended protocol ($n = 3$ in duplicate or triplicate).

2.5. Scanning electron microscopy

Scanning electron microscopy was used to examine the surface topography of brain, spinal cord, and UBM-ECM hydrogels. Five hundred micron thick hydrogels were prepared and then fixed in cold 2.5% glutaraldehyde (Electron Microscopy Sciences, Hatfield, PA) for 24 h followed by three 30 min washes in 1× PBS. Hydrogels were dehydrated in a graded series of alcohol (30, 50, 70, 90, 100% ethanol) for 30 min per wash, and then placed in 100% ethanol overnight at 4 °C. Hydrogels were washed 3 additional times in 100% ethanol for 30 min each and critical point dried using a Leica EM CPD030 Critical Point Dryer (Leica Microsystems, Buffalo Grove, IL, USA) with carbon dioxide as the transitional medium. Hydrogels were then sputter-coated with a 4.5 nm thick gold/palladium alloy coating using a Sputter Coater 108 Auto (Cressington Scientific Instruments, UK) and imaged with a JEOL JSM6330f scanning electron microscope (JEOL, Peabody, MA, USA).

2.6. Turbidity gelation kinetics

Turbidimetric gelation kinetics were determined as previously described [37]. The pre-gel solution was diluted to 6 mg/mL and maintained on ice at 4 °C until placed into a 96 well plate (100 μL/well). The plate was immediately transferred to a spectrophotometer (Molecular Devices) preheated to 37 °C, and absorbance was measured at 405 nm every 2 min for 50 min. Normalized absorbance was calculated using Equation (1) and then used to calculate the following parameters: time required to reach 50% and 95% maximum absorbance was denoted as $t_{1/2}$ and t_{95}, respectively, the lag phase, t_{lag}, calculated by extrapolating the linear portion of the curve, and the turbidimetric speed, S, of gelation was determined by calculating the growth portion slope of the curve normalized to absorbance [20]. The assay was repeated three times with independent samples in triplicate.

$$\text{Normalized Absorbance} = \frac{A - A_0}{A_{max} - A_0} \quad (1)$$

2.7. Rheological measurements

The pH of the ECM digest was neutralized to 7.4 and diluted to 4, 6, or 8 mg ECM/ml. The diluted pre-gel solution was then placed on a 40 mm parallel plate rheometer (AR 2000, TA Instruments) at 1 Pa stress and 10 °C to ensure even distribution and the liquidity of the pre-gel solutions between the plates. A dynamic time sweep was run with the parameters of 5% strain (with the exception of spinal cord ECM gel at 8 mg/mL, which was run with 0.5% strain), 1 rad/s (0.159 Hz) and rapidly increasing temperature from 10 °C to 37 °C to induce gelation as indicated by a sharp increase and plateauing of the storage modulus (G'), and the loss modulus (G'') ($n = 3$ per gel per concentration).

2.8. N1E-115 ECM cytocompatibility and two-dimensional neurite extension

N1E-115 mouse neuroblastoma cells (ATCC No. CRL 2263), a commonly used experimental cell line to examine neurotrophic potential and differentiation [33,34], were cultured in DMEM (Sigma) with 10% fetal bovine serum (FBS; Thermo Fisher Scientific, Waltham MA, USA)/1% pen/strep (Sigma) at a concentration of 100,000 cells per well in 12 well plate prior to the addition of ECM. B-ECM, SC-ECM, or UBM-ECM digest was added after cell attachment at a concentration of 100 μg ECM/mL. Following 18–24 h in culture with ECM, the medium was removed and 4 μM calcein-AM and 4 μM ethidium homodimer-1 was added to each well to evaluate cytotoxicity. Live cells that hydrolyze membrane-permeable calcein-AM, but not ethidium homodimer-1, fluoresce in green and dead cells that bind and activate ethidium homodimer-1, but not calcein-AM, fluoresce in red.

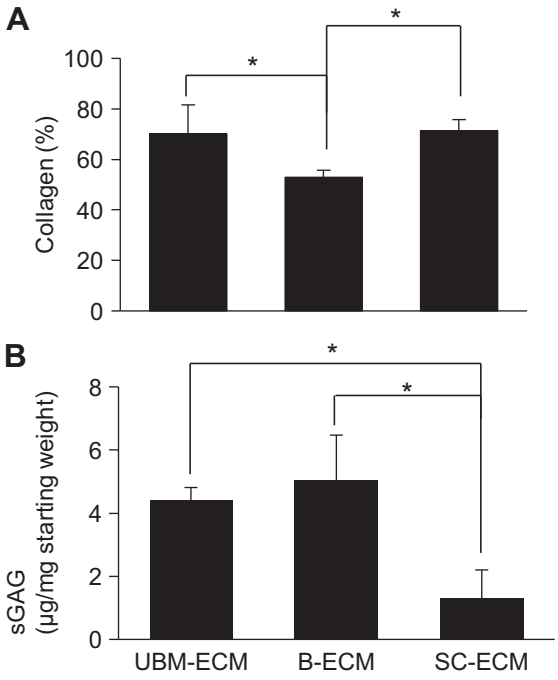

Fig. 1. Collagen and sGAG composition in B-ECM and SC-ECM scaffolds. (A) SC-ECM contains a significantly higher percentage of collagen than B-ECM. (B) B-ECM contains a significantly higher concentration of sGAGs than SC-ECM.

The effects of the B-ECM, SC-ECM, and UBM-ECM pre-gel digest upon N1E-115 neurite outgrowth were independently evaluated and used as an indicator of neurotrophic potential of the remaining bioactive molecules in ECM materials after enzymatic degradation. N1E-115 cells in DMEM with 10% FBS/1%pen strep were seeded at a density of 5000 cells/well in a 24 well plate. After incubation for 24 h, the media was removed and replaced with DMEM with 2.5% FBS, which promoted low levels of neurite extension and allowed changes in response to ECM to be quantified. Neutralized ECM pre-gel solutions at concentrations of 10 μg/mL and 100 μg/mL were added after cell attachment and cells were incubated for 48 h. N1E-115 cells were fixed with 2% paraformaldehyde for 20 min at room temperature. Attached cells were stained with DAPI for nuclei and Alexa Fluor phalloidin 488 (Invitrogen) for F-actin filaments. Three images at 200× magnification were taken per well. The number of cells with neurite extensions were manually counted. The longest neurite of each cell was measured in pixels using ImageJ (NIH). The outgrowth assay was repeated six times per condition. Neurites were denoted as cell processes that extended a minimum length of twice the diameter of the cell body. Image stacks were imported into Imaris software (Bitplane, South Windsor CN, USA) for 3-D visualization.

2.9. Neurite extension in three-dimensional culture

N1E-115 cells were maintained in 10% FBS DMEM media at 37 °C. B-ECM, SC-ECM, or UBM-ECM hydrogels (1 ml) were cast with a cell density of 500,000 cells/hydrogel and a concentration of 6 mg ECM/ml and after gelation for 1 h at 37 °C in a non-humidified incubator. All hydrogels were then cultured for 24 h in DMEM supplemented with 10% FBS/1% pen/strep. Serum concentration was reduced to 0% FBS and cells cultured for an additional 2 or 7 days. The hydrogels were then fixed with 4% paraformaldehyde (Fisher), stained for F-actin, and imaged using multiphoton confocal microscopy to visualize three-dimensional cell morphology inside the hydrogel scaffolds.

Hydrogels cultured with N1E-115 cells were stained with 0.1% Alexa Fluor 488 Phalloidin (Invitrogen) for 2 h and submerged in PBS solution in a hanging drop slide and coverslipped. To visualize neurite outgrowth in three dimensions, the slide was mounted beneath an Olympus FV1000 multiphoton system. The system was equipped with a Chameleon ultra-diode-pumped laser, and a 25× XL Plan N objective with a N.A. of 1.05 and a field of view of 500 μm. The excitation wavelength was chosen at 830 nm at a 6% laser transmissivity. The sampling speed was set to 2 μs/pixel with a 2 line Kalman filter, and the scanning had an incremental z-step of 1 μm. Image stacks were then compiled into a maximum intensity z-projection in ImageJ.

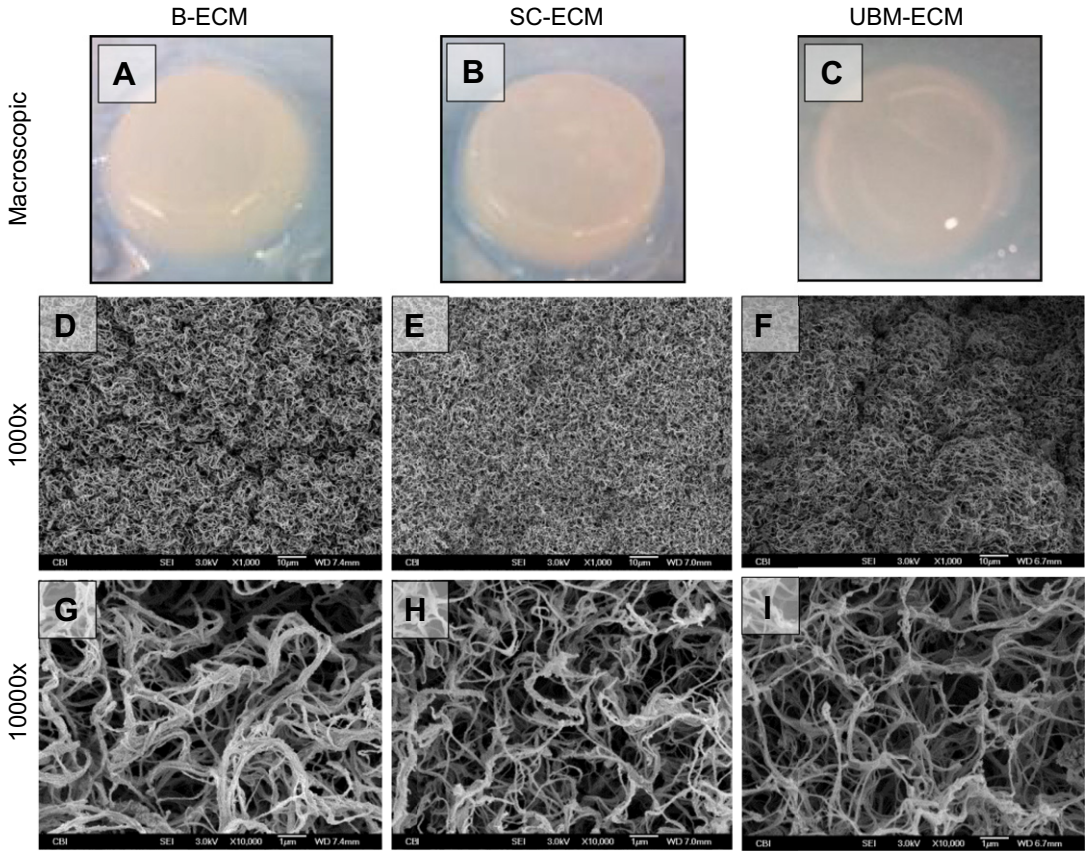

Fig. 2. B-ECM, SC-ECM, and UBM-ECM hydrogels and their respective scanning electron micrographs (6 mg/mL). (A) B-ECM hydrogel; (B) SC-ECM hydrogel; (C) UBM-ECM hydrogel; (D) B-ECM 1000×; (E) SC-ECM 1000×; (F) UBM-ECM 1000×; (G) B-ECM 10,000×; (H) SC-ECM 10,000×; (I) UBM-ECM 10,000×.

2.10. Statistical analysis

An independent Student's *t*-test was used to compare the effect of ECM pre-gel digests on N1E-115 cell differentiation to the effect of the no ECM control ($p < 0.05$). A one-way ANOVA was used for all other comparisons ($p < 0.05$). All statistical analysis methods used SPSS Statistical Analysis Software (SPSS, IBM, Chicago, IL, USA).

3. Results

3.1. Collagen and sGAG quantification

Collagen concentration of B-ECM was 537.5 ± 26.9 μg collagen/mg dry weight, which was less than SC-ECM and UBM-ECM at 703.2 ± 47.3 and 702.5 ± 113.5 μg collagen/mg dry weight, respectively ($p < 0.01$) (Fig. 1A). B-ECM and UBM-ECM had a higher sGAG concentration, 5.1 ± 1.4 ($p < 0.009$) and 4.4 ± 0.4 ($p < 0.02$) μg sGAG/mg dry weight, respectively, compared to SC-ECM, which was 1.3 ± 0.9 μg sGAG/mg dry weight (Fig. 1B).

3.2. Qualitative assessment

B-ECM, SC-ECM, and UBM-ECM pre-gel solutions polymerized to form a hydrogel at physiologic pH (7.4) and temperature (37 °C). Qualitatively, SC-ECM hydrogels were more rigid than B-ECM and UBM-ECM hydrogels (Fig. 2A–C). SEM micrographs showed dense, moderately organized collagen fibrils in B-ECM, SC-ECM, and UBM-ECM hydrogels (Fig. 2D–I). B-ECM contained the thickest fibrils (Fig. 2G), while SC-ECM hydrogels contained the most dense arrangement of fibrils (Fig. 2H). SC-ECM and UBM-ECM hydrogels contained moderately organized collagen fibers, while B-ECM contained dense clusters of randomly distributed collagen fibers.

3.3. Turbidimetric gelation kinetics

The gelation kinetics between hydrogel forms of B-ECM, SC-ECM, and UBM-ECM were evaluated using a normalized absorbance (Fig. 3A) to define the lag phase, times to reach half and 95% of the final turbidity, and speed to reach complete gelation using

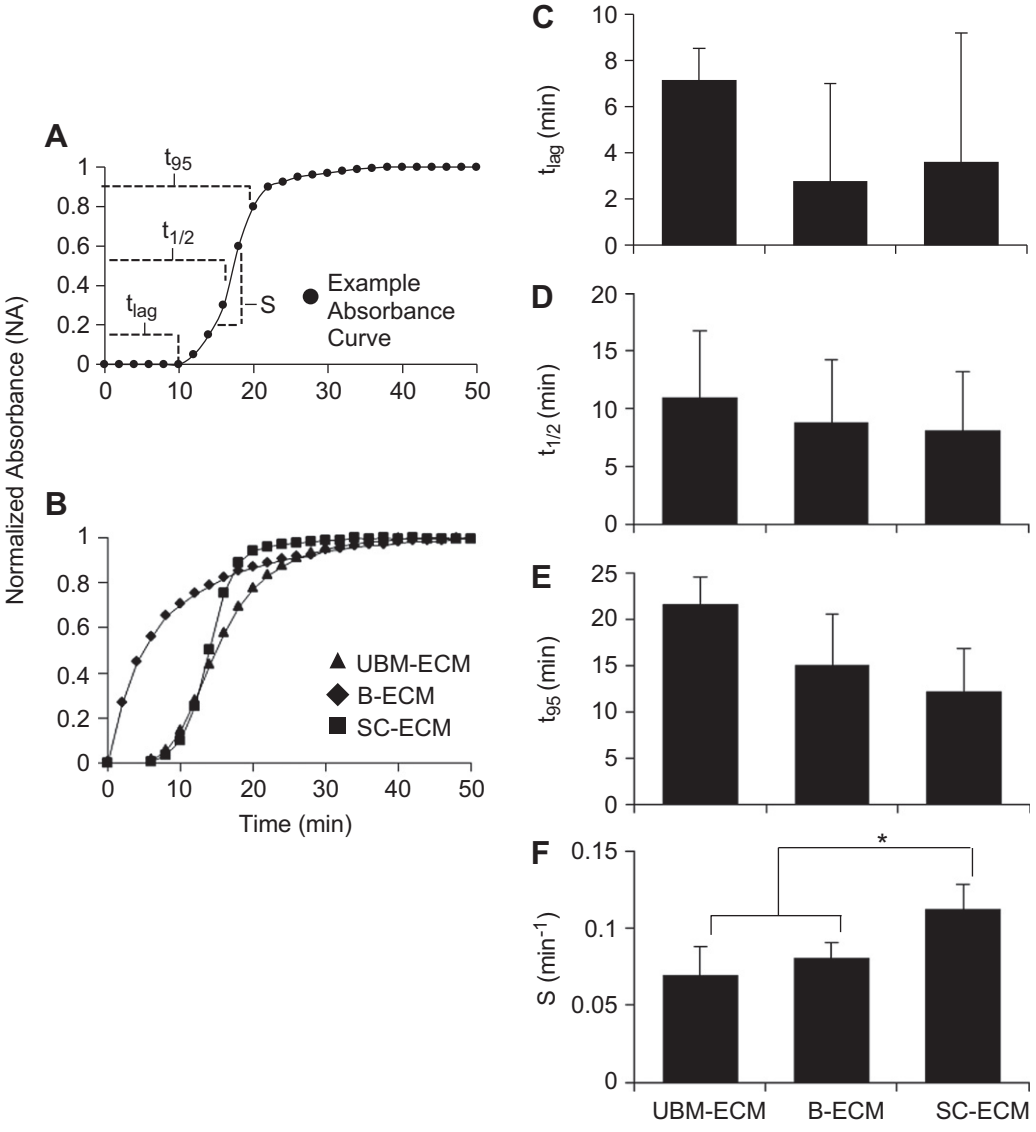

Fig. 3. B-ECM and SC-ECM representative turbidimetric and normalized turbidimetric curves. (A) Example absorbance curve and the metrics analyzed. (B) Normalized absorbance for B-ECM (diamonds), SC-ECM (squares), and UBM-ECM (triangles). (C) Lag time comparison for B-ECM, SC-ECM, and UBM-ECM. (D) Time to 50% complete gelation for B-ECM, SC-ECM, and UBM-ECM. (E) Time to 95% complete gelation for B-ECM, SC-ECM, and UBM-ECM. (F) Velocity to complete gelation for B-ECM, SC-ECM, and UBM-ECM following the lag time.

Table 2
Summary of rheologic and turbidity values for B-ECM, SC-ECM, and UBM-ECM.

Rheology	B-ECM (average (STDEV))			SC-ECM (average (STDEV))			UBM-ECM (average (STDEV))		
	4 mg	6 mg	8 mg	4 mg	6 mg	8 mg	4 mg	6 mg	8 mg
Storage modulus (G'; Pa)	20.3 (16.0)	49.9 (16.8)	61.8 (11.0)	138.5* (33.8)	235.5 (63.1)	757.0* (74.9)	11.43 (4.9)	72.78 (2.2)	143.8 (84.1)
Loss modulus (G''; Pa)	2.6 (1.9)	9.4 (4.6)	10.2 (1.8)	16.3* (4.9)	37.5* (11.4)	93.6* (10.9)	1.4 (0.6)	10.14 (0.5)	19.3 (12.3)
Complete gelation (Time; min)	34.8 (28.9)	2.4 (1.3)	8.3 (2.8)	11.7 (5.63)	7.0 (3.6)	28.97 (4.7)	52.5 (2.2)	8.47 (1.7)	19.8 (19.1)

Turbidity	B-ECM (average (STDEV))	SC-ECM (average (STDEV))	UBM-ECM (average (STDEV))
	6 mg	6 mg	6 mg
Speed (S; min^{-1})	0.8 (0.1)	0.11 (0.02)	0.07 (0.02)
50% gelation ($t_{1/2}$; min)	8.9 (5.4)	8.2 (5.1)	11.0 (5.8)
95% gelation (t_{95}; min)	15.1 (5.5)	12.2 (4.6)	21.6 (2.9)
Lag phase (t_{lag}; min)	2.8 (4.2)	3.6 (5.6)	7.2 (1.4)

* Indicates statistical significance at $p < 0.05$ when one group is statistically different from the other two.

turbidimetric gelation kinetics as previously described (Table 2) [20,37]. Turbidimetric gelation kinetics showed a sigmoidal shape for SC-ECM and UBM-ECM hydrogels, whereas B-ECM showed an exponential shape (Fig. 3B). Differences observed in kinetic curve shapes translated to a longer lag phase (t_{lag}; Fig. 3C) for UBM-ECM hydrogels (7.2 ± 1.4 min) than B-ECM (28 ± 4.2 min) or SC-ECM hydrogels (3.6 ± 5.6 min). The time required to reach half of the final turbidity ($t_{1/2}$; Fig. 3D) was also longer for UBM-ECM (11.0 ± 5.8 min) than B-ECM (8.9 ± 5.4 min) or SC-ECM hydrogels (8.2 ± 5.1 min). The time required to reach 95% of the final turbidity (t_{95}; Fig. 3E) was also longer for UBM-ECM hydrogels (21.6 ± 2.9 min) compared to B-ECM (15.1 ± 5.5 min) and SC-ECM hydrogels (12.2 ± 4.6 min). The velocity to complete gelation (S; Fig. 3F) was faster for SC-ECM hydrogels (0.11 ± 0.02 min^{-1}) compared to B-ECM (0.08 ± 0.01 min^{-1}) and UBM-ECM (0.07 ± 0.02 min^{-1}) ($p < 0.05$). These results suggest that during hydrogel assembly, SC-ECM hydrogels reach the steady state plateau faster than B-ECM or UBM-ECM hydrogels.

3.4. Rheologic measurements

The storage modulus (G') and the loss modulus (G'') for B-ECM, SC-ECM, and UBM-ECM hydrogels changed over time as the sample temperature increased rapidly from 10 °C to 37 °C. Sigmoidal storage and loss moduli curves showed increased maximum storage modulus, maximum loss modulus, and time to complete gelation as concentration increased (Fig. 4A–C). SC-ECM hydrogels had the largest storage modulus at all hydrogel concentrations (Fig. 4D). At 8 mg/mL, the storage modulus for SC-ECM, 757.0 ± 74.8 Pa, was greater than both UBM-ECM and B-ECM ($p < 0.05$), which showed storage moduli of 143.8 ± 84.1 Pa and 61.8 ± 11.0 Pa, respectively. While B-ECM hydrogels have lower storage moduli than SC-ECM and UBM-ECM hydrogels, B-ECM hydrogels at a concentration of 6 mg/mL reached the steady state plateau in 2.4 ± 1.3 min; a time that was faster than UBM-ECM and SC-ECM, which had times of 8.5 ± 1.7 min and 7.0 ± 3.6 min, respectively. Table 2 summarizes the storage modulus, loss

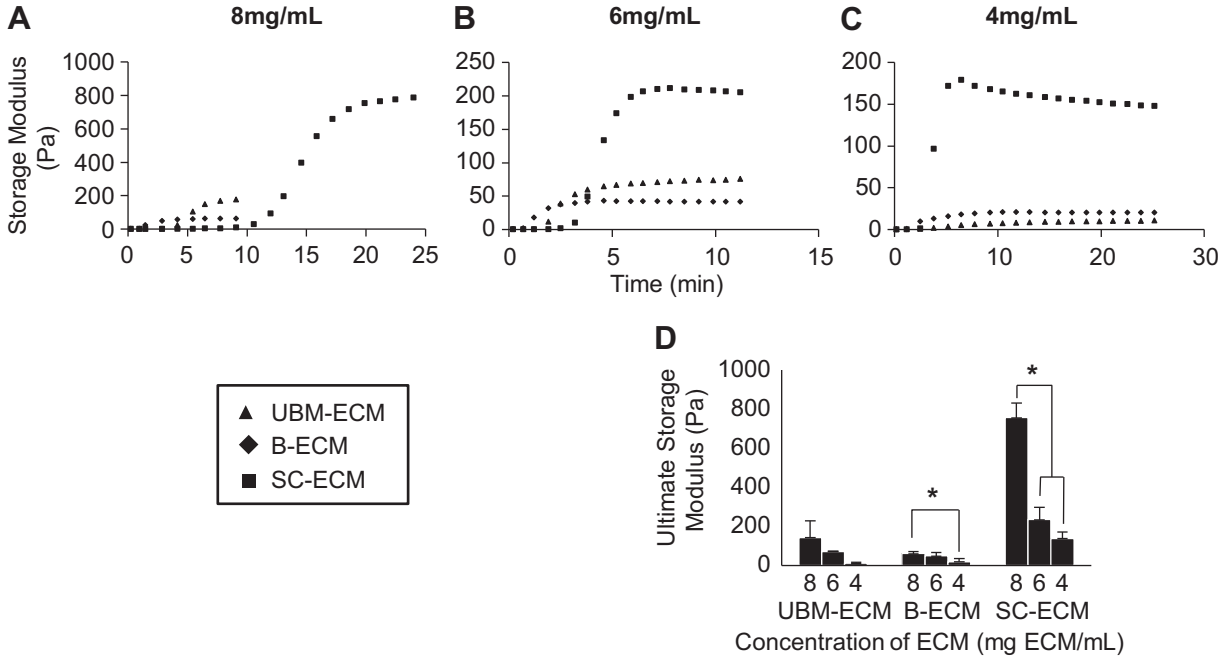

Fig. 4. Representative rheologic gelation kinetics for B-ECM and SC-ECM hydrogels (4, 6, and 8 mg/mL). G' represents the storage modulus and G'' represents the loss modulus. SC-ECM is significantly stiffer than B-ECM at each hydrogel concentration. (A) Storage modulus time sweep for B-ECM, SC-ECM, and UBM-ECM at 8 mg/mL. (C) Storage modulus time sweep for B-ECM, SC-ECM, and UBM-ECM at 6 mg/mL. (C) Storage modulus time sweep for B-ECM, SC-ECM, and UBM-ECM at 4 mg/mL. (D) Final storage modulus for B-ECM, SC-ECM, and UBM-ECM at each concentration. * Indicates statistical significance of $p < 0.05$.

modulus, and time to complete gelation for each ECM hydrogel at concentrations of 4, 6, and 8 mg/mL.

3.5. N1E-115 ECM cytocompatibility and two-dimensional neurite extension

The live/dead assay showed all ECMs to be non-cytotoxic for N1E-115 cells (Fig. S1). B-ECM, SC-ECM, and UBM-ECM pre-gel solutions at concentrations of 10 and 100 μg ECM/mL increased the number of cells extending neurites (differentiated cells) compared to cells cultured without ECM digest. At 100 μg ECM/mL, SC-ECM digest promoted the highest percentage of differentiation, with 69.7 ± 14.0% of the cells extending neurites, whereas UBM-ECM and B-ECM promoted, 57.4 ± 12.1% and 54.3 ± 11.7% respectively. At 10 μg and 100 μg ECM/mL, B-ECM, SC-ECM, and UBM-ECM increased the percentage of cells with neurite extensions compared to the buffered control; however B-ECM was the only scaffold that showed an increase in neurite extension length for both 10 and 100 μg ECM/ml compared to cells cultured without ECM (Fig. 5).

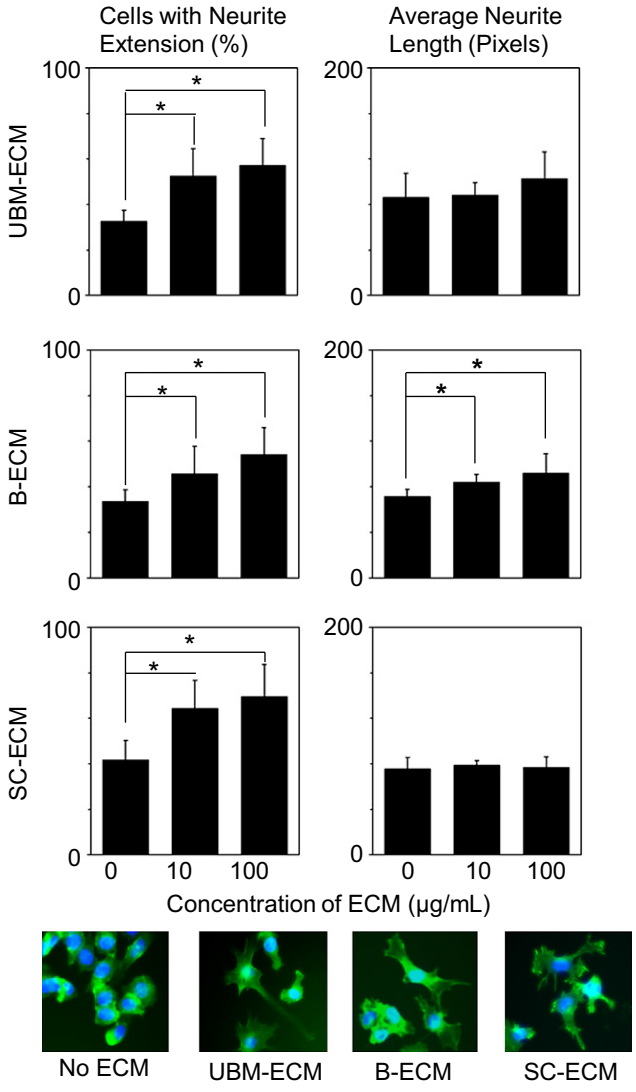

Fig. 5. B-ECM and SC-ECM pre-gel solutions increase the number of cells with neurite extensions. All scaffolds show a dose dependent increase for the number of cells with neurite extension, while only B-ECM shows a dose dependent increase in neurite length with increasing concentrations of ECM. * Indicates statistical significance of $p < 0.05$.

3.6. Neurite extension in three-dimensional culture

B-ECM, SC-ECM, and UBM-ECM supported the formation of three-dimensional neurite extensions at 2 and 7 days following removal of serum (Fig. 6). N1E-115 cells seeded in B-ECM hydrogels promoted a short arborizing growth pattern at two days, while SC-ECM and UBM-ECM hydrogels induce unipolar extensions. By 7-days, all ECM hydrogels promoted unipolar or bipolar extensions (Fig. 6).

4. Discussion

The present study shows that biologic scaffolds derived from porcine brain and spinal cord can be processed to form hydrogels that retain selected ECM-specific constituents. At comparable ECM concentrations, these hydrogel forms of CNS-ECM have distinctive composition and biomechanical properties. Furthermore, CNS-ECM hydrogels are cytocompatible, promote N1E-115 cell differentiation, and support three-dimensional neurite extension.

The mechanical properties of SC-ECM hydrogels are similar to those previously shown to support neuronal differentiation of stem cells (0.1–1 kPa) [38]. It is therefore plausible that the rheologic and turbidimetric properties of CNS-ECM hydrogels can be used to influence the differentiation of endogenous or therapeutically administered stem cells following CNS injury [38]. The gelation kinetics and storage moduli of CNS-ECM hydrogels can be manipulated to a certain extent by varying ECM concentrations, such that following polymerization a hydrogel could be made with tailored in vivo pre-polymerization lag time, final storage modulus, and rate of polymerization [39]. Altering these parameters may enhance not only the ability of the gels to modulate stem cell behaviors, but also the cell and drug delivery properties of CNS-ECM hydrogels [40,41].

It is logical that the distinctive collagen and sGAG concentrations play a role in ECM hydrogel gelation and rheologic properties; therefore, quantification of the collagen and sGAG concentrations provides valuable insight. Furthermore, the collagen monomers aggregate and self-assemble into thin filaments that can then crosslink into collagen fibers that interweave with themselves and other ECM components to contribute to hydrogel formation [42]. The shorter polymerization time and smaller storage modulus of B-ECM hydrogel compared to SC-ECM hydrogel may result from the higher sGAG concentration found in B-ECM hydrogels. Concentration of sGAGs has been shown to alter gelation kinetics and mechanical properties of hydrogels [43,44]. While UBM-ECM hydrogel has a similar concentration of sGAGs compared to B-ECM hydrogel, the increased storage modulus could be due to a possible increased ratio of collagen I to collagen III in UBM-ECM hydrogel [45,46]. The increased storage modulus of SC-ECM hydrogel compared to UBM-ECM hydrogel may result from relatively low sGAG concentration found in SC-ECM. Although collagen composition of B-ECM contains approximately 50% collagen, native brain contains very limited amounts of ECM components including collagen [47]. It should be noted that the percent collagen described herein represents a percentage of the isolated ECM, rather than a percentage of the mass of the intact brain prior to decellularization. While collagen and sGAGs affect hydrogel mechanical properties, further studies are needed to determine those additional molecules present in the ECM hydrogels that may contribute to polymerization.

Both composition and material properties of the CNS derived hydrogels are distinct from a hydrogel derived from a non-CNS tissue source (UBM-ECM) [20]. The unique ECM composition of different organs [48,49], suggests that ECM scaffolds derived from the same tissue type as that of the injury site may contain bioactive components uniquely able to induce constructive remodeling of

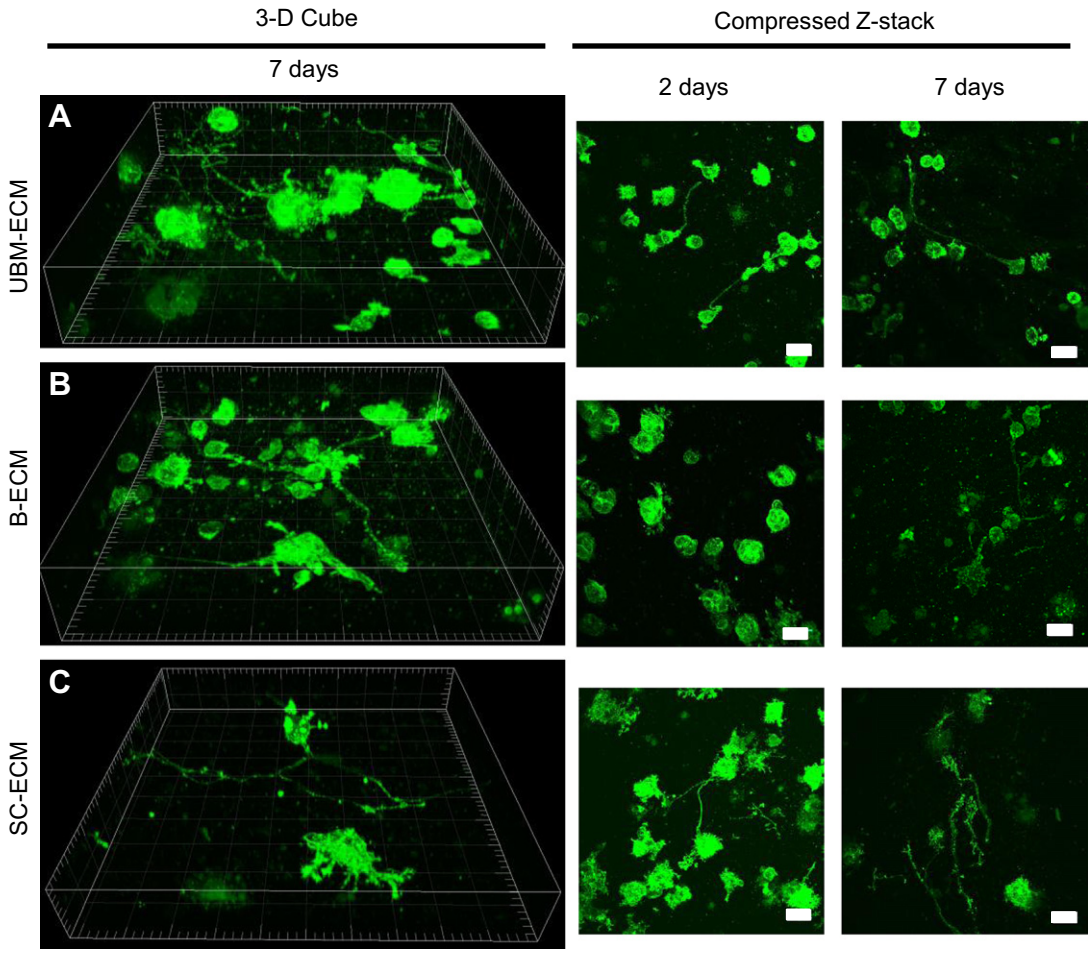

Fig. 6. Neurite extension in B-ECM, SC-ECM, and UBM-ECM in 6 mg/mL hydrogels in a 3-D cube or compressed Z-stack. (A) N1E-115 cell extension following 7 days culture in B-ECM in 3-D cube. (B) N1E-115 cell extension following 7 days culture in SC-ECM in 3-D cube. (C) N1E-115 cell extension following 7 days culture in UBM-ECM in 3-D cube. The compressed Z-stack shows B-ECM has short arborizing extensions at two days, while SC-ECM and UBM-ECM have uni- or bi-polar extensions. At 7 days all ECM hydrogels support uni- or bi-polar N1E-115 cell extensions. For 3-D cubes the major tick mark represents 50 μm and the minor tick mark represents 10 μm. For the Z-stacks the scale bar represents 50 μm.

that tissue type. An array of proteins and peptides will be generated during ECM solubilization [9,20] that is reflective of the molecular profile of the organ from which the ECM is derived. Thus, a hydrogel derived from solubilized and digested CNS-ECM will contain a unique composition of molecular constituents resembling those found within the ECM of healthy CNS tissue. The bioactive factors retained in the ECM hydrogels in the present study are neurotrophic as evident by the formation of N1E-115 cell neurite extensions when cultured in the presence of ECM digests. In addition, the present study shows that B-ECM hydrogels increase the length of N1E-115 neurite extensions in two-dimensional culture. This effect is not seen in UBM-ECM or SC-ECM digest, a possible indication of a tissue-specific effect of B-ECM upon these brain derived cells [33,50].

5. Conclusions

B-ECM and SC-ECM hydrogels, while derived by similar decellularization methods from their source tissue, each have a unique biochemical composition, mechanical properties, and neurotrophic potential. The increase in neurite length for N1E-115 cells in response to B-ECM suggests a tissue-specific effect of B-ECM hydrogels on a brain derived cell line. Each ECM elicited unique cell responses as demonstrated by neurotrophic potential in their solubilized form and support of considerable three-dimensional neurite growth and extension in their re-polymerized hydrogel forms; this finding suggests that the molecular constituents of the source ECM play an important role in the bioactivity of these scaffolds. Support of three-dimensional neurite extension by CNS-ECM hydrogels also suggests the possibility that these hydrogels provide the scaffolding necessary to promote in vivo axonal repair and warrants further study.

Acknowledgments

Christopher Medberry was partially supported by the NIH-NHLBI training grant (T32-EB001026) entitled “Cellular Approaches to Tissue Engineering and Regeneration.” Peter Crapo was partially supported by an Ocular Tissue Engineering and Regenerative Ophthalmology (OTERO) Fellowship from the Louis J. Fox Center for Vision Restoration (a joint program of UPMC and the University of Pittsburgh). Matthew Wolf was partially supported by the NIH-NHLBI training grant (T32-HL76124-6) entitled “Cardiovascular Bioengineering Training Program.” Christopher Carruthers was partially supported by the National Science Foundation (NSF) Graduate Research Fellowship. Shailesh Nagarkar was partially supported by a grant from the National Science Foundation (NSF-0932901). Vineet Agrawal was supported by a NIH F30 training grant (1F30-HL102990 (VA)). The authors would like to thank

Deanna Rhoads, Gregory A. Gibson, the McGowan Histology Center for histologic section preparation, and Biologic Imaging at the University of Pittsburgh for access to imaging facilities.

Appendix A. Supplementary data

Supplementary data related to this article can be found at http://dx.doi.org/10.1016/j.biomaterials.2012.10.062.

References

[1] Badylak SF, Vorp DA, Spievack AR, Simmons-Byrd A, Hanke J, Freytes DO, et al. Esophageal reconstruction with ECM and muscle tissue in a dog model. J Surg Res 2005;128(1):87–97.
[2] Badylak SF, Hoppo T, Nieponice A, Gilbert TW, Davison JM, Jobe BA. Esophageal preservation in five male patients after endoscopic inner-layer circumferential resection in the setting of superficial cancer: a regenerative medicine approach with a biologic scaffold. Tissue Eng Part A 2011; 17(11–12):1643–50.
[3] Wood JD, Simmons-Byrd A, Spievack AR, Badylak SF. Use of a particulate extracellular matrix bioscaffold for treatment of acquired urinary incontinence in dogs. J Am Vet Med Assoc 2005;226(7):1095–7.
[4] Sutherland RS, Baskin LS, Hayward SW, Cunha GR. Regeneration of bladder urothelium, smooth muscle, blood vessels and nerves into an acellular tissue matrix. J Urol 1996;156(2 Pt 2):571–7.
[5] Zantop T, Gilbert TW, Yoder MC, Badylak SF. Extracellular matrix scaffolds are repopulated by bone marrow-derived cells in a mouse model of Achilles tendon reconstruction. J Orthop Res 2006;24(6):1299–309.
[6] Iannotti JP, Codsi MJ, Kwon YW, Derwin K, Ciccone J, Brems JJ. Porcine small intestine submucosa augmentation of surgical repair of chronic two-tendon rotator cuff tears. A randomized, controlled trial. J Bone Jt Surg Am 2006; 88(6):1238–44.
[7] Robinson KA, Li J, Mathison M, Redkar A, Cui J, Chronos NA, et al. Extracellular matrix scaffold for cardiac repair. Circulation 2005;112(Suppl. 9):I135–43.
[8] Ota T, Gilbert TW, Schwartzman D, McTiernan CF, Kitajima T, Ito Y, et al. A fusion protein of hepatocyte growth factor enhances reconstruction of myocardium in a cardiac patch derived from porcine urinary bladder matrix. J Thorac Cardiovasc Surg 2008;136(5):1309–17.
[9] Reing JE, Zhang L, Myers-Irvin J, Cordero KE, Freytes DO, Heber-Katz E, et al. Degradation products of extracellular matrix affect cell migration and proliferation. Tissue Eng Part A 2009;15(3):605–14.
[10] Crisan M, Yap S, Casteilla L, Chen CW, Corselli M, Park TS, et al. A perivascular origin for mesenchymal stem cells in multiple human organs. Cell Stem Cell 2008;3(3):301–13.
[11] Badylak SF, Valentin JE, Ravindra AK, McCabe GP, Stewart-Akers AM. Macrophage phenotype as a determinant of biologic scaffold remodeling. Tissue Eng Part A 2008;14(11):1835–42.
[12] Brown BN, Valentin JE, Stewart-Akers AM, McCabe GP, Badylak SF. Macrophage phenotype and remodeling outcomes in response to biologic scaffolds with and without a cellular component. Biomaterials 2009;30(8):1482–91.
[13] Beattie AJ, Gilbert TW, Guyot JP, Yates AJ, Badylak SF. Chemoattraction of progenitor cells by remodeling extracellular matrix scaffolds. Tissue Eng Part A 2009;15(5):1119–25.
[14] Brennan EP, Tang XH, Stewart-Akers AM, Gudas LJ, Badylak SF. Chemoattractant activity of degradation products of fetal and adult skin extracellular matrix for keratinocyte progenitor cells. J Tissue Eng Regen Med 2008;2(8): 491–8.
[15] Agrawal V, Tottey S, Johnson SA, Freund JM, Siu BF, Badylak SF. Recruitment of progenitor cells by an extracellular matrix cryptic peptide in a mouse model of digit amputation. Tissue Eng Part A 2011;17(19–20):2435–43.
[16] Agrawal V, Brown BN, Beattie AJ, Gilbert TW, Badylak SF. Evidence of innervation following extracellular matrix scaffold-mediated remodelling of muscular tissues. J Tissue Eng Regen Med 2009;3(8):590–600.
[17] Crapo PM, Wang Y. Small intestinal submucosa gel as a potential scaffolding material for cardiac tissue engineering. Acta Biomater 2010;6(6):2091–6.
[18] Dequach JA, Lin JE, Cam C, Hu D, Salvatore MA, Sheikh F, et al. Injectable skeletal muscle matrix hydrogel promotes neovascularization and muscle cell infiltration in a hindlimb ischemia model. Eur Cell Mater 2012;23:400–12.
[19] Seif-Naraghi SB, Salvatore MA, Schup-Magoffin PJ, Hu DP, Christman KL. Design and characterization of an injectable pericardial matrix gel: a potentially autologous scaffold for cardiac tissue engineering. Tissue Eng Part A 2010;16(6):2017–27.
[20] Freytes DO, Martin J, Velankar SS, Lee AS, Badylak SF. Preparation and rheological characterization of a gel form of the porcine urinary bladder matrix. Biomaterials 2008;29(11):1630–7.
[21] Sellaro TL, Ranade A, Faulk DM, McCabe GP, Dorko K, Badylak SF, et al. Maintenance of human hepatocyte function in vitro by liver-derived extracellular matrix gels. Tissue Eng Part A 2010;16(3):1075–82.
[22] Wolf MT, Daly KA, Brennan-Pierce EP, Johnson SA, Carruthers CA, D'Amore A, et al. A hydrogel derived from decellularized dermal extracellular matrix. Biomaterials 2012;33(29):7028–38.
[23] Crapo PM, Medberry CJ, Reing JE, Tottey S, van der Merwe Y, Jones KE, et al. Biologic scaffolds composed of central nervous system extracellular matrix. Biomaterials 2012;33(13):3539–47.
[24] Sellaro TL, Ravindra AK, Stolz DB, Badylak SF. Maintenance of hepatic sinusoidal endothelial cell phenotype in vitro using organ-specific extracellular matrix scaffolds. Tissue Eng 2007;13(9):2301–10.
[25] Price AP, England KA, Matson AM, Blazar BR, Panoskaltsis-Mortari A. Development of a decellularized lung bioreactor system for bioengineering the lung: the matrix reloaded. Tissue Eng Part A 2010;16(8):2581–91.
[26] Cortiella J, Niles J, Cantu A, Brettler A, Pham A, Vargas G, et al. Influence of acellular natural lung matrix on murine embryonic stem cell differentiation and tissue formation. Tissue Eng Part A 2010;16(8):2565–80.
[27] Bible E, Dell'Acqua F, Solanky B, Balducci A, Crapo PM, Badylak SF, et al. Non-invasive imaging of transplanted human neural stem cells and ECM scaffold remodeling in the stroke-damaged rat brain by (19)F- and diffusion-MRI. Biomaterials 2012;33(10):2858–71.
[28] Boruch AV, Nieponice A, Qureshi IR, Gilbert TW, Badylak SF. Constructive remodeling of biologic scaffolds is dependent on early exposure to physiologic bladder filling in a canine partial cystectomy model. J Surg Res 2010;161(2): 217–25.
[29] Turner NJ, Yates Jr AJ, Weber DJ, Qureshi IR, Stolz DB, Gilbert TW, et al. Xenogeneic extracellular matrix as an inductive scaffold for regeneration of a functioning musculotendinous junction. Tissue Eng Part A 2010;16(11): 3309–17.
[30] Kumar A, Godwin JW, Gates PB, Garza-Garcia AA, Brockes JP. Molecular basis for the nerve dependence of limb regeneration in an adult vertebrate. Science 2007;318(5851):772–7.
[31] Kumar A, Nevill G, Brockes JP, Forge A. A comparative study of gland cells implicated in the nerve dependence of salamander limb regeneration. J Anat 2010;217(1):16–25.
[32] Brockes JP. The nerve dependence of amphibian limb regeneration. J Exp Biol 1987;132:79–91.
[33] Tuttle JB, Richelson E. Ionic excitation of a clone of mouse neuroblastoma. Brain Res 1975;84(1):129–35.
[34] Dan C, Nath N, Liberto M, Minden A. PAK5, a new brain-specific kinase, promotes neurite outgrowth in N1E-115 cells. Mol Cell Biol 2002;22(2):567–77.
[35] Freytes DO, Badylak SF, Webster TJ, Geddes LA, Rundell AE. Biaxial strength of multilaminated extracellular matrix scaffolds. Biomaterials 2004;25(12): 2353–61.
[36] Piper DW, Fenton BH. pH stability and activity curves of pepsin with special reference to their clinical importance. Gut 1965;6(5):506–8.
[37] Gelman RA, Williams BR, Piez KA. Collagen fibril formation. Evidence for a multistep process. J Biol Chem 1979;254(1):180–6.
[38] Engler AJ, Sen S, Sweeney HL, Discher DE. Matrix elasticity directs stem cell lineage specification. Cell 2006;126(4):677–89.
[39] Aguado BA, Mulyasasmita W, Su J, Lampe KJ, Heilshorn SC. Improving viability of stem cells during syringe needle flow through the design of hydrogel cell carriers. Tissue Eng Part A 2012;18(7–8):806–15.
[40] Hoffman AS. Hydrogels for biomedical applications. Adv Drug Deliv Rev 2002; 54(1):3–12.
[41] Agashi K, Chau DY, Shakesheff KM. The effect of delivery via narrow-bore needles on mesenchymal cells. Regen Med 2009;4(1):49–64.
[42] Pedersen JA, Swartz MA. Mechanobiology in the third dimension. Ann Biomed Eng 2005;33(11):1469–90.
[43] Obrink B. The influence of glycosaminoglycans on the formation of fibers from monomeric tropocollagen in vitro. Eur J Biochem 1973;34(1):129–37.
[44] Stuart K, Panitch A. Influence of chondroitin sulfate on collagen gel structure and mechanical properties at physiologically relevant levels. Biopolymers 2008;89(10):841–51.
[45] Birk DE, Silver FH. Collagen fibrillogenesis in vitro: comparison of types I, II, and III. Arch Biochem Biophys 1984;235(1):178–85.
[46] Stuart K, Panitch A. Characterization of gels composed of blends of collagen I, collagen III, and chondroitin sulfate. Biomacromolecules 2009; 10(1):25–31.
[47] Ruoslahti E. Brain extracellular matrix. Glycobiology 1996;6(5):489–92.
[48] Daley WP, Peters SB, Larsen M. Extracellular matrix dynamics in development and regenerative medicine. J Cell Sci 2008;121(Pt 3):255–64.
[49] Adams JC, Watt FM. Regulation of development and differentiation by the extracellular matrix. Development 1993;117(4):1183–98.
[50] Amano T, Richelson E, Nirenberg M. Neurotransmitter synthesis by neuroblastoma clones (neuroblast differentiation-cell culture-choline acetyltransferase-acetylcholinesterase-tyrosine hydroxylase-axons-dendrites). Proc Natl Acad Sci U S A 1972;69(1):258–63.